CFD Analysis of Hydraulic Oscillator for Flow Separation Control

Ryuto Yoshida*, Wataru Kobayashi*, and Seiichiro Tanibuchi*

*Graduate School of Science and Engineering, Okayama University of Science, Okayama, Japan
*E-mail: r23smt2mn@ous.jp, w-kobayashi@ous.ac.jp, r24smh1jt@ous.jp

Abstract

The objective of this study is to control the separation flow of ship. Previous studies on ship separation control has carried out passive methods and active methods. These studies have some issue for example energy and another conditions. There, this study focuses on fluidics as one of the passive methods, applied to oscillators using switching elements. However, previous study has been clarified that a bit error between design to actual of chamber and orifice make difference oscillation. Therefore, this study proposes integrated type oscillator that it integrates chamber, orifice and switching element. Also, this study analyzes the reduction of fluid resistance around the ship using this oscillator. Based on this research background, the study first analyzes the proposed oscillator's characteristics, focusing on parameters like orifice and chamber volume, which influence the oscillation period and frequency. By adjusting the output port diameter (1.4 to 2.8 mm), the oscillation period inside the chamber is halved. Also, increasing the chamber volume raises the average pressure and the maximum pressure difference during oscillation. However, the effectiveness of this approach in reducing fluid resistance around the ship remains unclear. To investigate further, this study created a ship model, and separation behavior is analyzed with the oscillator installed.

Keywords: Flow separation control, CFD, Hydraulic oscillator, Fluidics

1 Introduction

In Japan, maritime transportation plays a crucial role in international trade, with ships accounting for 99% of overseas cargo transport [1]. Therefore, improving the transport efficiency of ships is essential and various studies have been conducted to improve this efficiency. These include optimization of operation routes [2], enhancement of engine power of ships [3], and reduction of fluid resistance around ships. In optimization of operation routes, optimization of operation routes has been proposed to quantitatively estimate changes in route selection when the ship size increases. This estimation uses simulation models that reproduce the current container cargo volume. In studies for fluid resistance reduction, the focus has been on the environment around the ship and the reduction of fluid friction [4]. One focusing on the environment around the ship is the development of special ship bottom paint to reduce resistance caused by bio-fouling. Thus, various approaches aim to improve transport efficiency. Among these, this study focuses specifically on methods to reduce fluid resistance around ships.

1.1 Fluid separation and turbulence

This study focuses on methods to reduce fluid resistance. Therefore, attention is given to fluid separation, which is one of the causes of fluid resistance in ships. As shown in Figure 1, fluid separation refers to the phenomenon in which a fluid flowing along the surface of an airfoil gradually decreases in velocity due to viscous friction with the surface. As the fluid moves toward the rear of the object, it encounters increasing difficulty in maintaining its flow against the opposing pressure. Eventually, the fluid separates from the surface and flows away. Moreover, the flow with reduced velocity may even acquire a reverse velocity, changing direction due to friction with the separated flow.

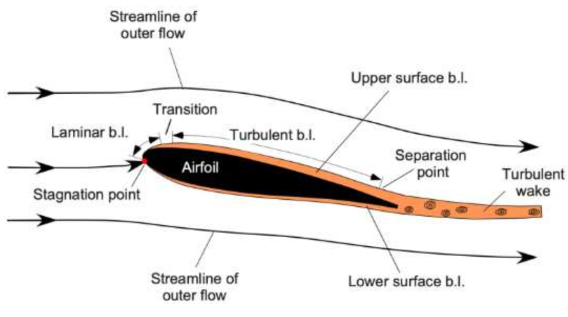

Figure 1: Flow patterns around airfoil [5]

This separation results in a pressure difference between the front and rear of the object, which generates resistance as the object moves forward [5] [6]. This phenomenon-induced resistance is considered an important issue in maritime vessels. Also, the point where the fluid velocity becomes zero and the flow separates from the object's surface is called the separation point. To reduce fluid resistance, a method is to intentionally disturb the laminar flow near the separation point, which helps to move the separation point downstream [7]. For example, aircraft wings use flaps as shown in Figure 2, and propellers positioned at the rear of the aircraft create a suction effect to move the separation point [8]. In ships, one method to reduce frictional resistance involves introducing microbubbles along the ship surface as shown in Figure 3. These microbubbles create a lubricating layer between the ship and the surrounding water, effectively decreasing viscous drag and improving fuel efficiency. It has been demonstrated that the use of microbubbles can reduce wall shear stress by up to 30% [9]. However, to achieve a more efficient reduction in frictional resistance, ships need to specifically design built-in microbubble generators. Additionally, it is essential to assess the effects of microbubble generator in the propeller area to ensure optimal performance. Beyond passive techniques, active control methods utilize external power sources, such as electricity, to reduce fluid resistance and improve transport efficiency. However, The efficiency improves only by the amount of energy subtracted from the power due to the reduction of fluid resistance. In some cases, these methods may offer only marginal benefits or even lead to increased energy consumption.

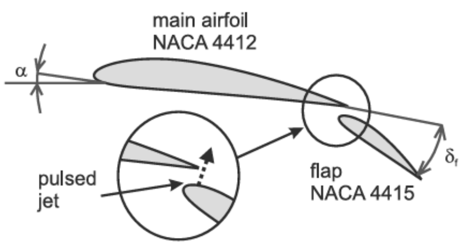

Figure 2: Schematic diagram of flap surface moving device [8]

Figure 3: Overview of ship and built-in micro bubble generator [9]

In contrast, passive methods, which reduce fluid resistance without using energy, have been gaining much more attention. Some of them include the dimples on golf balls as shown in Figure 4, and vortex generators on the surfaces of cars and airplanes as shown in Figure 5 [10]. The dimples on the ball create turbulence near the separation point, preventing flow separation during flight and enhancing the ball flight distance. In related study, it shows dimpled golf balls experience lower drag due to delayed flow separation at the rear end, allowing them to travel farther. The dimples cause the boundary layer to transition from laminar to turbulent flow, similar to vortex generators. This turbulent flow stays attached longer, delaying flow separation and reducing form drag. As a result, total drag, which includes form drag and skin friction, is minimized, improving the ballâs distance [11] .

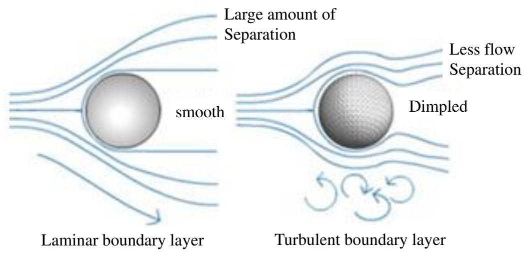

Figure 4: Simulation results of velocity vector distribution of golf ball (left: w/o dimple, right: w/ dimple) [11]

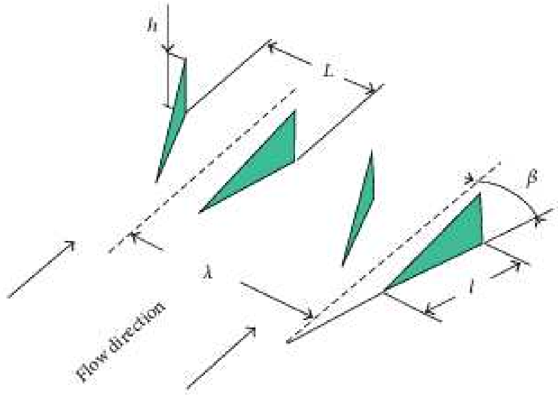

Figure 5: Vortex generator geometry [10]

1.2 Fluidics

One of the passive methods is an application of fluidics. Fluidics is a technology that controls fluids by utilizing phenomenon generated by the fluid itself, without mechanical moving parts. Since it controls the fluid solely through its own properties, it has been extensively studied for its potential use in environments where electronic devices are difficult to apply. Figure 6 shows an application of fluidics for medical fields, which called micro fluidics [12] [13].

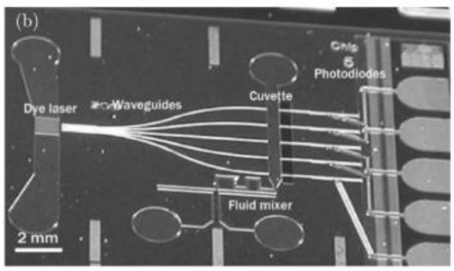

Figure 6: Micro fluidics [13]

Fluidics are highly reliable and durable because they do not have any mechanical moving parts. However, due to the constant flow, they have a large energy loss and lower response time compared with typical electric systems [14]. Fluidic elements that can perform some functions such as OR, AND, flip-flops, and Switching have been developed [15]. By performing drug synthesis on microchannels carved into silicon or glass, the amount of samples and reagents can be significantly reduced, offering benefits such as time savings and reduced waste disposal. On the other hand, due to the phenomenon occurring in microscopic environments, challenges include the difficulty of measuring temperature and flow rate, as well as the need for technology to inject fluids into the microchannels [16]. Although the devices are manufactured by inserting channels, it has become possible to produce devices, including channels, using 3D printers with advancements in technology. Additionally, improvements in the precision of channel carving enable the creation of smaller channels and components. As a result, manufacturers can decrease costs, and they can also achieve the miniaturization of components. Thus, fluidics is expected to have various elements and applications, and useful for passive detachment suppression for ships as well.

1.3 Fluidic switching elements

In this study, the focus is on a fluid switching device that can change the flow path using only fluid. Also, we are considering a valveless switching system with the aim of realizing a purely aqua-driven system in the future. However, as demonstrated in this paper, this oscillator also has the potential to reduce fluid resistance. Therefore, to reduce the fluid resistance of ships, this study is developing an oscillator that is driven solely by fluid, as described below. First, this section presents the structure of the fluid switching element and describes its operating principle. Then, the effective design revealed by previous research is discussed [17]. A fluidic switching element has three types of ports: an input port, a control port, and an output port, as shown in Figure 7. The roles of these ports are as follows: the input port supplies pressure, the control port determines the direction of output, and the output port is responsible for the final output of pressure and flow velocity. After the control port determines the output direction of the main flow, the Coanda effect draws the main flow toward the side wall due to the negative pressure generated between the side wall and the main flow. This mechanism helps maintain the flow path. As shown in Figure 8, the operating principle

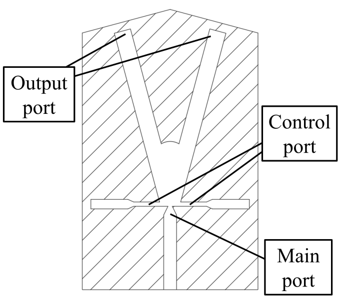

Figure 7: Structure of fluidic switching element

of the fluid switching device is explained as follows: 1) The main jet flow entering from the input port flows toward the left and right output ports. 2) By applying flow from the left and right control ports, the main jet is deflected toward the sidewalls. 3) The deflected main jet maintains its direction due to the Coanda effect. Through these operations, switching is made possible using only fluid.

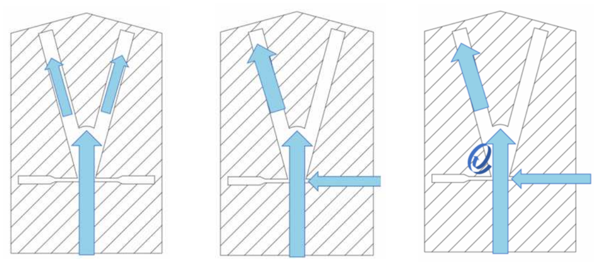

Figure 8: Operating principle of switching element

In the optimal shape for switching, however, various factors such as the diameter of the split, the distance to the split, the diameter of the input port, and the diameter of the output port all have an impact. Therefore, in previous studies, analyses were conducted on the switching and maintenance of flow paths, clarifying the effects of the design parameters of switching elements and confirming the feasibility of a switchable design. This analysis focuses on three parameters shown in Figure 9 (L_s: split distance, H: offset distance, and θ: sidewall inclination angle) which are considered to be important factors influencing the switching of flow channels and the maintenance of flow direction.

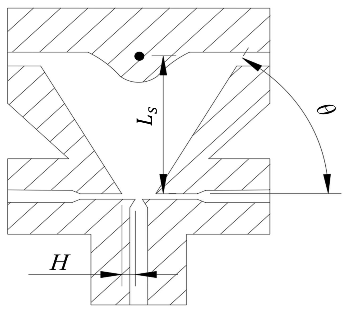

Figure 9: Structure of fluidic switching element

2 Fluidic oscillator using switching element

Fluidic switching elements, which is previously analyzed in our studies , have been applied in various fields. One of them is the fluidic oscillator, which is possible to oscillate by connecting a volumetric chamber and an orifice to a fluid switching element as shown in the figure 10. In a related study, a fluidic oscillator was applied to artificial hearts as a medical device. The study noted that periodic pressure fluctuations strongly influence the frequency and amplitude of pressure fluctuations, especially when the orifice diameter is reduced. On the other hand, the study pointed out a concern that, depending on the structure of the element, pressure may switch to the opposite direction before reaching the calculated pressure [18]. This study investigates the use of this fluidic oscillators to prevent fluid separation around the ship.To understand the characteristics of the fluidic oscillator, This study constructed an experimental setup. As shown in Figure 11, the experimental setup consists of a fluidic switching element, a pressure chamber, and a pressure sensor (PSE560-02, SMC Corporation). The supply pressure is set to 280 kPa corresponding to the tap water pressure in our laboratory. Also, this study adjusted the orifice diameter in the center of the oscillator by controlling the switching element's control port. Figure 12 shows the experimental results, showing oscillation frequencies of up to 150 Hz depending on the pressure chamber volume and orifice diameter. However, both the frequency and amplitude of pressure fluctuation exhibited instability. This instability suggests that parameters such as the pressure chamber volume, tube volume, and orifice diameter have a significant impact on the oscillation characteristics. Small discrepancies in the design can strongly influence the oscillation behavior.

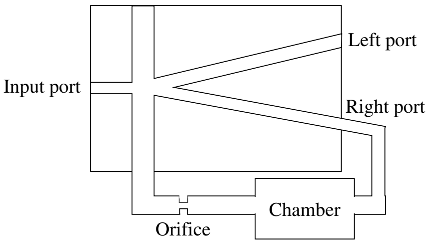

Figure 10: Schematic diagram of conventional oscillator

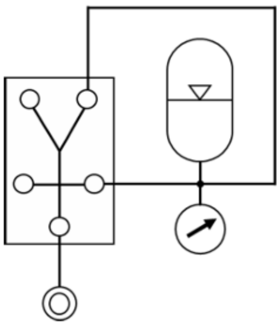

Figure 11: Experiment setup for conventional oscillator

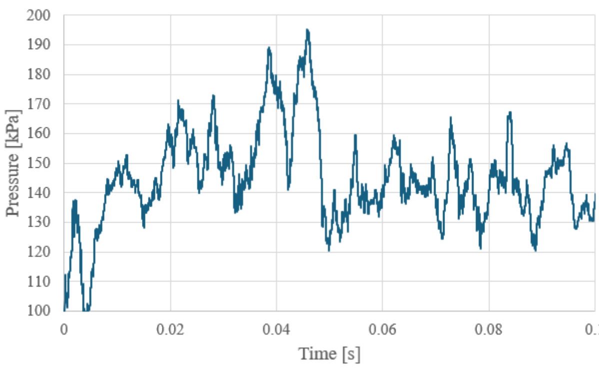

Figure 12: Measured pressure response in oscillator chamber

2.1 Integrated type fluidic oscillator

As mentioned in the previous section, even slight design discrepancies can make it difficult to operate the oscillator when manufactured according to theoretical specifications. To address this issue, this study proposes an integrated type fluidic oscillator that takes into account of the effects of the chamber, tubes, and orifices. Figure 13 shows the design of the proposed integrated type fluidic oscillator.

Building upon a conventional oscillator design, the configuration consists of a fluidic switching element, left and right pressure chambers, and an orifice connecting the right pressure chamber to the right control port. The proposed oscillator has following two key characteristics: 1) the right pressure chamber connects to the control port, and 2) the pressure chamber and orifice are integrally molded. By integrally molding the pressure chamber and orifice with the fluidic element, the impact of these components on oscillation can be minimized. Figure 14 shows the operating principle of the oscillator. The process is as follows: 1) Fluid is supplied from the input port and flows into both the left and right pressure chambers, 2) The internal pressure in the pressure chambers, 3) Flow occurs from the right control port, directing the main flow to the left pressure chamber, 4) Coanda effect occurs along the side wall of the oscillator, maintaining the flow direction, 5) The internal pressure of the left pressure chamber increases and the flow to the right pressure chamber decreases, 6) The internal pressure of the right pressure chamber decreases and also the flow from the right control port decreases, 7) The main flow switches from the left to the right pressure chamber. By repeating this process, passive oscillation can be achieved without any external power sources.

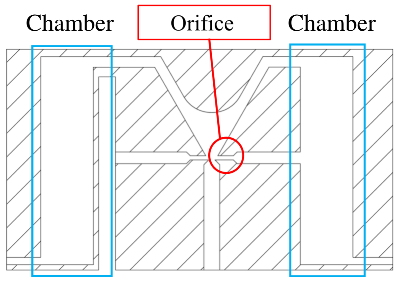

Figure 13: Structure of integrated type fluidic oscillator

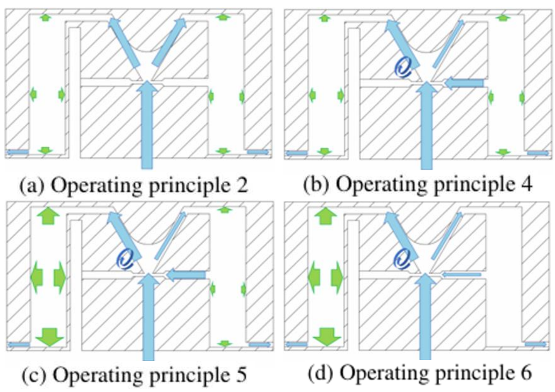

Figure 14: Operating principle of proposed oscillator

2.2 Analysis of oscillator: Initial conditions

This section evaluates the oscillation performance of the proposed oscillator and analyzes the effect of design parameters of the oscillator for its oscillation behavior. The analyzed oscillator has dimensions of 77.5 mm in length and 43 mm in width. Table 1 lists the design parameters while Figure 15 visually illustrates these parameters. In these analyses, internal pressure of chambers p_1, p_2 and flow velocity of output ports u_1, u_2 are measured. The first analysis focuses on the output port diameters, T_R and T_L, of the oscillator, as these diameters influence the oscillation period. Another key parameter is the thickness D, which affects the amplitude of pressure fluctuation. Regarding the inlet flow conditions, both the output port and the left control port of the oscillator open to the atmosphere, and supply pressure for the oscillator is 300 kPa. Additionally as shown in Figure 16, the mesh number of the oscillator set to 640,000, with further refinement by a factor of 1/8 at the center of the oscillator. Also, this study needs to observe a detailed understanding of the internal flow within the oscillator, particularly phenomena such as the coanda effect. For this reason, this study adopted a CFD-based approach.

Table 1: Design parameters of proposed oscillator for analysis

Variable	Symbol	Value
Chamber width	W_L and W_R	15 mm
Output port diameter	T_L and T_R	1.4 mm
Oscillator thickness	D	10 mm

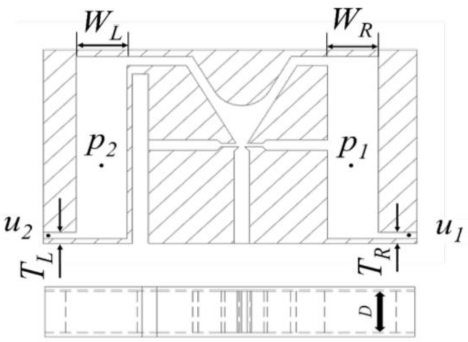

Figure 15: Design parameters of proposed oscillator

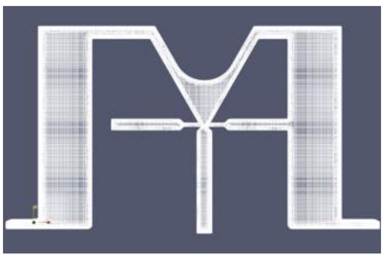

Figure 16: Analysis model of proposed oscillator

Figures 17 and 18 shows the analysis results for the design parameters listed in Table 1. Figure 17 describes the velocity distribution at 0.1 and 0.44 s, respectively. The flow velocity from the input port can switch from the left pressure chamber to the split section. Figure 18 shows the time response of p_1 and p_2. The average pressure in the pressure chamber is 90 kPa and the oscillation period is 0.1 s, and the maximum pressure difference is approximately 25 kPa. Additionally, from Figures 18, it was confirmed that oscillation is possible, as the internal pressure is fluctuating at the left output port.

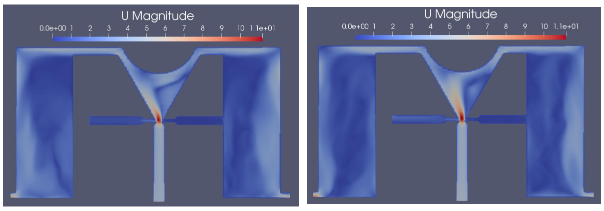

Figure 17: Velocity distribution of proposed oscillator (left: 0.1 s, right: 0.44 s)

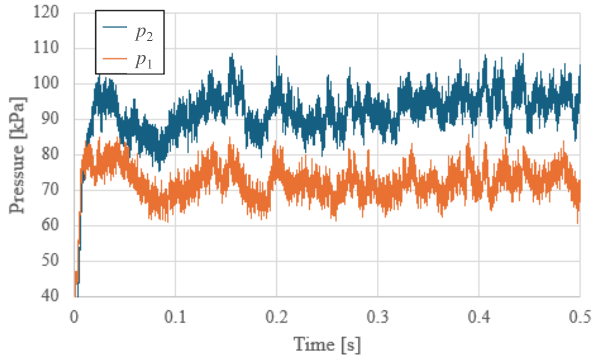

Figure 18: Pressure response of chambers in proposed oscillator

2.3 Analysis of oscillator: Output port diameter

First, the output port diameter of the oscillator, which affects the oscillation period, is analyzed. Figure 19 shows the results when W_L is changed from 1.4 to 2.8 mm. Top-left to bottom-right of Figure 19 show the velocity distribution at 0.1, 0.3, 0.4 and 0.5 s respectively. As shown in Figure 19, the flow velocity oscillates from the input port towards both the left and right pressure chambers.

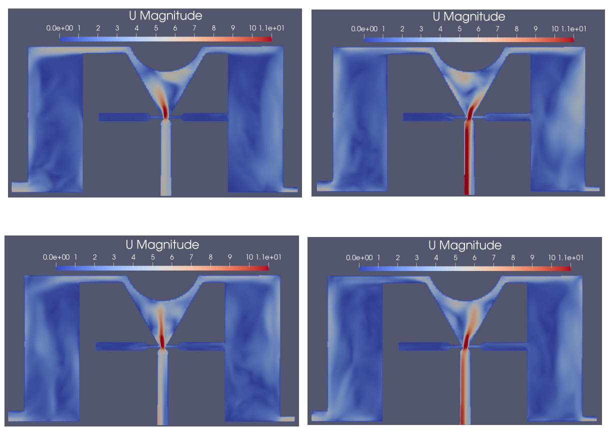

Figure 19: Velocity distribution of proposed oscillator (top-left: 0.1 s, top-right: 0.3 s, bottom-left: 0.4 s, bottom-right: 0.5 s)

Figure 20 describes the time response of internal pressure of the chambers at p_1 and p_2 when T_L is 1.4 and 2.8 mm. Figure 20 shows that the average pressure inside the left chamber is approximately 30 kPa at the case that the left output port diameter is 2.8 mm. Also, by performing analysis of frequency components using FFT (Fast Fourier Transform), the frequency component was confirmed to be 20 Hz, as shown in the figure 21. This means 60 kPa reduction in average pressure compared to the previous case with the diameter of 1.4 mm, and the oscillation period is halved. Oscillations between the left and right pressure chambers and the center split can be observed when the pressure difference between the left and right chambers reversed, and when the pressure difference decreased to 15 kPa. Therefore, it can be concluded that the output port diameter significantly influences the oscillation period and plays a crucial role in determining the pressure difference between the left and right pressure chambers.

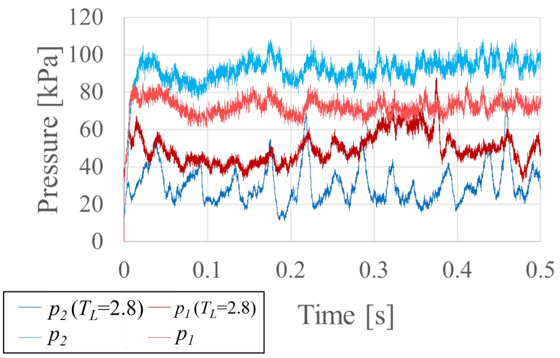

Figure 20: Comparison of internal pressure of chambers

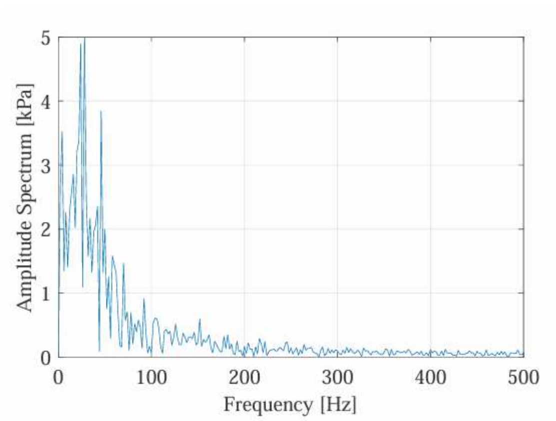

Figure 21: Frequency component analysis result

Figures 22 and 23 shows the results when T_R is changed from 1.4 to 2.8 mm. Figure 22 describes the velocity distribution at 0.1, 0.19, 0.31, and 0.42 s, while Figure 23 shows the time response of pressure at p_1 and p_2. As seen in Figure 22, the flow velocity from the input port primarily oscillates towards the left pressure chamber and the center split. Figure 23 indicates that p_1 increases significantly by 0.03 s, after which oscillatory fluctuations are observed. This is thought to be due to the decreased flow towards the left pressure chamber and the relatively increased flow towards the right pressure chamber. These results suggest that varying the diameter of the right output port T_R affects the oscillation.

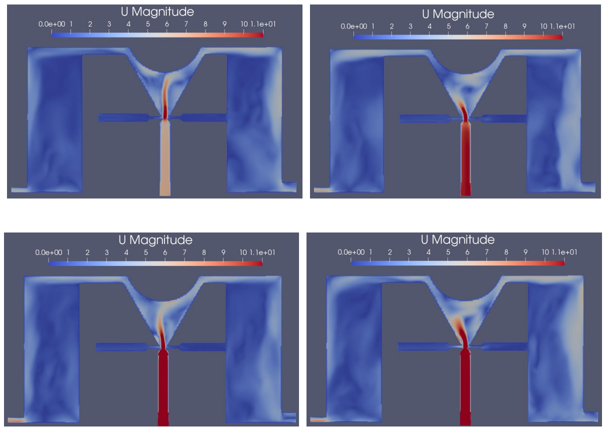

Figure 22: Velocity distribution of proposed oscillator with T_L: 2.8 mm (top-left: 0.1 s, top-right: 0.3 s, bottom-left: 0.4 s, bottom-right: 0.5 s)

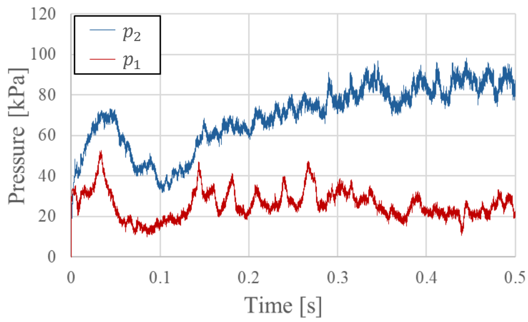

Figure 23: Pressure response of chambers in proposed oscillator ($T_R = 2.8$ mm)

2.4 Analysis of oscillator: Chamber volume

Next, this study focused on the chamber volume of the oscillator, which is thought to affect the amplitude of pressure fluctuation, and conducted analysis by varying several parameters. Figures 24 and 25 show the analysis results when the height D is changed from 10 to 15 mm. Figure 24 presents the flow velocity distribution inside the element at 0.1 and 0.3 s, respectively. Figure 25 shows the time response of pressure p_1 and p_2. As shown in Figure 24, the flow velocity from the input port moves towards the left chamber. On the other hand, no clear switching of flow direction to the right chamber is observed. In Figure 25, the average pressures in the left and right chambers are 75 and 60 kPa, respectively. The pressure difference between the maximum and minimum pressures is small and this indicates that the volume of the chambers significantly affects the amplitude of pressure fluctuation.

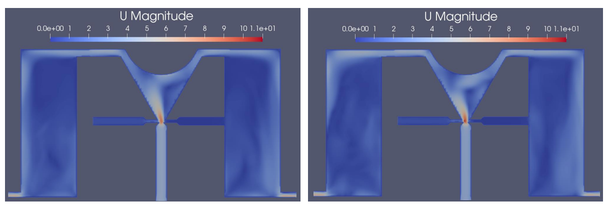

Figure 24: Velocity distribution of proposed oscillator with D: 15 mm (left: 0.1 s, right: 0.3 s)

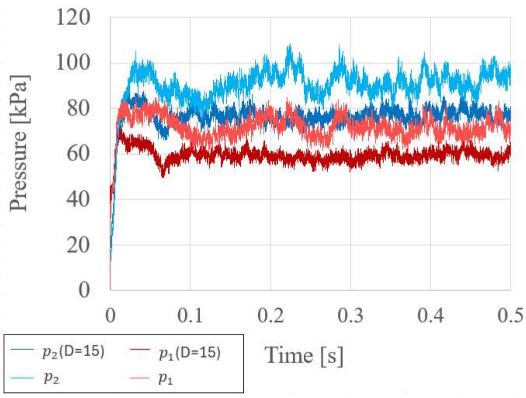

Figure 25: Pressure response of chambers in proposed oscillator (D =10, 15 mm)

Figures 26 and 27 show the analysis results when the pressure chamber height D is changed from 10 to 5 mm. Figure 26 presents the flow velocity distribution inside the element at 0.1 and 0.45 s, respectively. Figure 27 shows the time response of pressure p_1 and p_2. As shown in Figure 26, the flow continues towards the left chamber. The average pressure in the left chamber is 120 kPa, and the maximum differential pressure is 30 kPa. This clearly indicates that the volume of the chambers affects the amplitude of pressure fluctuation. Regarding the periodic oscillation, the period is faster compared to the period of previous oscillator with the height of 10 mm. This phenomenon is due to the reduced time required to accumulate pressure, as the volume of the chamber is decreased. From the results, it is evident that the diameter of the left output port in the oscillator affects the oscillation period.

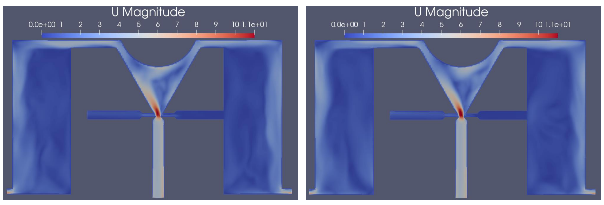

Figure 26: Velocity distribution of proposed oscillator with D: 5 mm (left: 0.1 s, right: 0.45 s)

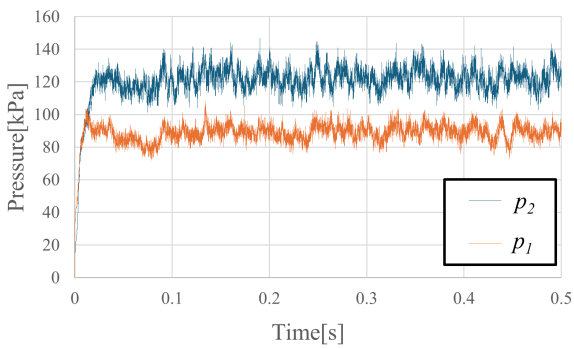

Figure 27: Pressure response of chambers in proposed oscillator (D = 5 mm)

3 Analysis of flow separation around ship

In this chapter, this study created a simple ship model and then CFD analysis shows its behavior when turbulent flow generated by the proposed oscillator is introduced around the ship model. This will help clarify the effective oscillation frequency for separation control of ships. The proposed oscillator is integrated at the separation point on the model shown in Figure 28. Figure 29b shows the created ship model, and its shape is taken from the A-A cross-section in Figure 29a. The model is 3.5 m in length, 1.6 m in width and 0.5 m in height.

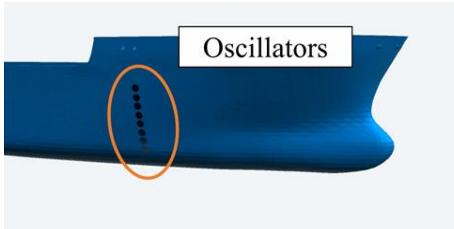

Figure 28: Image of oscillators arrangement at ship

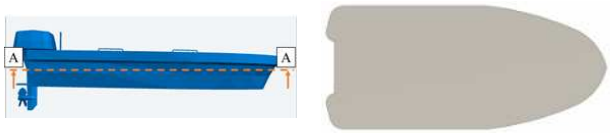

(a) Side view of ship *(b) Cross section view*

Figure 29: Analysis model of ship

3.1 Analysis of separation control without oscillator

To clarify the optimal oscillation for separation control, the first analysis is conducted on separation control for the conventional shape without the integrated oscillator. In this analysis, the applied turbulence model and sampling period are the same as those in the previous section. The mesh resolution is 640,000, with an additional 1/8 division around the separation point and a further 1/64 division around the output port of the oscillator. While this may seem relatively small, the mesh resolution around the injection point was additionally increased, and the analysis was performed again ant then no significant differences were observed. Therefore, this study believes that this simulation has sufficient validity. The cruising speed of the ship is 20.5 m/s. Figure 30 shows the analysis results and illustrates the velocity distribution in the X-direction which means heading direction of the ship. It is confirmed that the flow velocity around the ship decreases and spreads from near the ship side toward the rear of the ship. Additionally, the result of supplying a steady flow from the oscillator's output port, meaning it generates a steady flow instead of a periodic turbulent flow is shown in Figure 31. It illustrates the flow velocity distribution in the X-direction, where a negative flow velocity indicates movement toward the stern. The flow rate from the oscillator is 20.5 m/s and the oscillator applies only to the starboard side of the ship (bottom side), with no oscillator on the port side (top side). The decrease in flow velocity is mitigated on the starboard side compared to conventional flow, as shown in Figure 31, but no significant reduction in flow velocity occurs at the rear of the ship. Even with steady flow applied, separation fails to be sufficiently controlled.

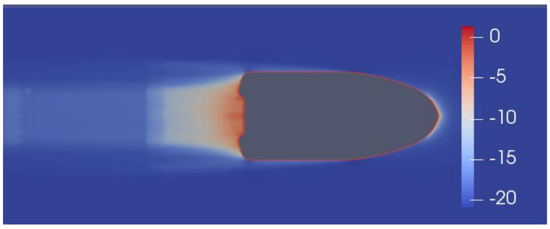

Figure 30: Velocity distribution (w/o oscillator)

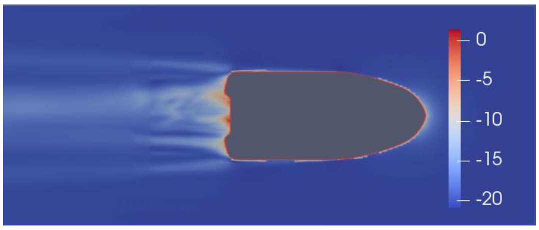

Figure 31: Velocity distribution (w/ steady flow)

3.2 Analysis of separation control with oscillator

In this section, to achieve flow separation control around the ship, the integrated oscillator is installed into the ship model, and analyses are conducted to evaluate its effect on flow separation. The optimal oscillation frequency for separation control is determined. This study draws on research related to aircraft wings, which encounter similar separation issues. In the studies, the concept of reduced frequency F^+, commonly used in aircraft wing separation control, is introduced. It is defined by following eq. (1)

$$F^+ = \frac{fl}{U} \tag{1}$$

where f is the oscillation frequency, l the characteristic length, and U the flow velocity. By adjusting this frequency, the effective oscillation frequency for separation control can be determined. However, the optimal reduced frequency varies depending on objectives and is often determined experimentally. Therefore, while referencing reduced frequency, this study investigates separation control around the ship using an integrated oscillator, examining the effects of oscillation frequencies of 1, 10, and 100 Hz. The ship model, analysis conditions, and flow boundary conditions are as same as those described above. First, an analysis is conducted with oscillation frequency of 1 Hz applied from the oscillator. Figure 32 illustrates the X-direction flow velocity distribution. The calculated F^+ at 1 Hz is 0.17, which is lower than the conventional optimal value for related studies. No significant difference in flow velocity is observed compared to the previous analysis shown in Figure 31. In addition, the maximum flow velocity around the port side of the ship is 16 m/s, while on the starboard side with oscillator, the maximum velocity remains approximately 16 m/s. These results suggest that a low F^+ is insufficient for effective flow separation control around the ship. Figure 33 illustrates the analysis results for oscillation frequency of 10 Hz along with the flow velocity distribution in the X-direction. The calculated F^+ at 10 Hz is 1.7, which corresponds to the conventional optimal value reported in related studies. Compared to the previous analysis shown in Figure 31, a reduction in flow velocity is observed and the maximum flow velocity on the starboard side of the ship is approximately 18 m/s. These results indicate that the given F^+ is effective for controlling flow separation around the ship. Figure 34 illustrates the analysis results for oscillation frequency of 100 Hz along with the flow velocity distribution in the X-direction. The calculated F^+ at 100 Hz is 17, which is larger than the conventional optimal value reported in related studies. As shown in Figure 34, however, the decrease in flow velocity is effectively mitigated with the maximum velocity of 18.5 m/s. The area where the flow velocity decreases near the rear of the ship seems to be smaller than the area of the previous analysis in Figure 31. Furthermore, a reduction in the area where the flow velocity significantly decreases in the wake of the ship can be observed. The analyses presented in this chapter demonstrate that the reduced frequency F^+ significantly influences flow separation control in ships. The observed discrepancy is likely attributable to the omission of fluid property considerations, such as viscosity differences between air and water, in the formulation of the reduced frequency. Further investigations that incorporate fluid-specific parameters are required to refine the flow separation control strategy for this application.

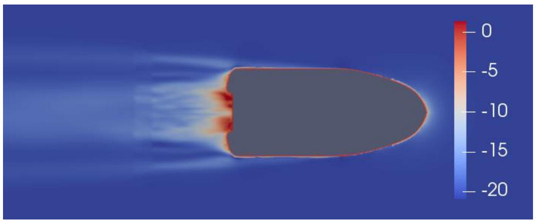

Figure 32: Simulation result of flow velocity of ship (1 Hz)

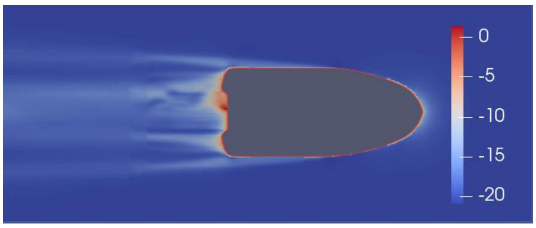

Figure 33: Simulation result of flow velocity of ship (10 Hz)

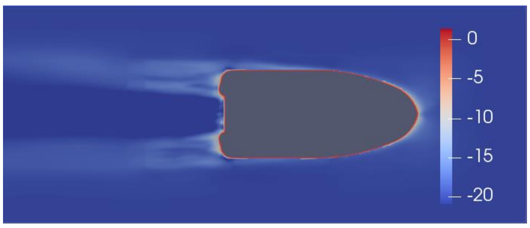

Figure 34: Simulation result of flow velocity of ship (100 Hz)

4 Conclusion

This study focuses on fluidic switching elements that can switch fluid paths using only fluid, with the aim of developing an oscillator that can be driven solely by fluid in order to reduce fluid resistance in ships. In previous fluidic oscillators using switching elements, oscillation occurred without external input due to the influence of chambers, tubes, and orifices. However, achieving the desired oscillation period and frequency was difficult due to small design errors in these components. Therefore, this study proposes an integrated fluidic oscillator that combines the chamber and tube into a single unit. Also, to evaluate the proposed oscillator and clarify the effects of various design parameters on oscillation, an analysis was conducted. Results showed that changing the diameter of the output port of each oscillator modifies the oscillation period, and adjusting the chamber volume changes the amplitude of pressure fluctuation. This enables the design of an oscillation period and frequency effective in reducing the fluid resistance of ships. While there have been numerous studies on the reduction of resistance through fluidic separation, there are few examples of study focused on ships. Therefore, this study aims to clarify the oscillations that are effective in reducing the fluid resistance of the ship. First, a simplified ship model was created, and through analysis, it was confirmed that separation occurs. For this analysis, this study focused on separation at a specific height on the ship. Next, this study assumed the installation of the oscillator at a part of the ship model and applied oscillations under specific conditions to analyze the separation behavior. The results of the analysis revealed that an oscillation period in the range of 10-100 Hz most effectively control separation. As future work, it is necessary to investigate the separation behavior at different heights of the ship and compare it with the current results. Furthermore, based on these analysis results, this study needs to design an oscillator with an optimal oscillation period for separation control and conduct a further analysis of the oscillation when input conditions are altered. Additionally, since this study mainly focuses on analysis, it will be important to verify the consistency with experimental results.

Nomenclature

Designation	Denotation	Unit
D	Oscillator thickness	mm
f	Oscillation frequency	Hz
F^+	Reduced frequency	-
H	Offset distance	mm
l	Characteristic length	m
L_s	Split distance	mm
p_1	Right chamber pressure	kPa
p_2	Left chamber pressure	kPa
T_L	Left output port diameter	mm
T_R	Right output port diameter	mm
θ	Sidewall inclination angle	degree
U	Flow velocity	m/s
u_1	Right outport pressure	kPa
u_2	Left outport pressure	kPa
W_L	Left chamber width	mm
W_R	Right chamber width	mm

Acknowledgments

Part of this work was supported by JSPS KAKENHI Grant Number JP21K14133.

References

[1] Trade Ministry of Economy and Industry. White paper on international economy and trade [outline]. 2020.

[2] Ryuichi SHIBASAKI and Tomihiro WATANABE. Future forecast of trade amount and international cargo flow in the apec region: An application of trade-logistics forecasting model. *Asian Transport Studies*, 2(2):194–208, 2012.

[3] Simone Lion, Ioannis Vlaskos, and Rodolfo Taccani. A review of emissions reduction technologies for low and medium speed marine diesel engines and their potential for waste heat recovery. *Energy Conversion and Management*, 207:112553, 2020.

[4] Liang Li, Heting Hong, Jingyi Cao, and Yange Yang. Progress in marine antifouling coatings: Current status and prospects. *Coatings*, 13(11):1893, 2023.

[5] J. G. Leishman. Introduction to aerospace flight vehicles. 2022.

[6] William S. Vorus. A theory for flow separation. *Journal of Fluid Mechanics*, 132:163–183, 1983.

[7] Dennis Bushnell. Separation control: Review. *Journal of Fluids Engineering*, 113, 04 1991.

[8] Ralf Petz and Wolfgang Nitsche. Active separation control on the flap of a two-dimensional generic high-lift configuration. *Journal of Aircraft - J AIRCRAFT*, 44:865–874, 05 2007.

[9] Ali Dogrul, Yasemin Arıkan Özden, and Fahri Çelik. A numerical investigation of air lubrication effect on ship resistance. *SMOOTH 2010*, 01 2010.

[10] Shi-bo Tao, Aiping Tang, Da-bo Xin, Ke-tong Liu, and Hong-fu Zhang. Vortex-induced vibration suppression of a circular cylinder with vortex generators. *Shock and Vibration*, 2016:1–10, 01 2016.

[11] Shabir Grover, B B Arora, Vaibhav Khanna, Tushar Kaushik, and Akhilesh Arora. International journal of advanced production and industrial engineering innovative design computational modelling analysis on drag reduction of bluff body using dimples. *International Journal of Advanced Production and Industrial Engineering*, pages 4–11, 01 2017.

[12] Vigneswaran Narayanamurthy, Z. E. Jeroish, K. S. Bhuvaneshwari, Pouriya Bayat, R. Premkumar, Fahmi Samsuri, and Mashitah M. Yusoff. Advances in passively driven microfluidics and lab-on-chip devices: a comprehensive literature review and patent analysis. *RSC Adv.*, 10:11652–11680, 2020.

[13] Henrik Bruus. *Theoretical microfluidics*, volume 18. Oxford university press, 2007.

[14] Kin Fong Lei. Microfluidic systems for diagnostic applications: A review. *Journal of laboratory automation*, 17(5):330–347, 2012.

[15] Animesh Pratap Singh, Marcel Tintelott, Elmira Moussavi, Sven Ingebrandt, Rainer Leupers, Xuan-Thang Vu, Farhad Merchant, and Vivek Pachauri. Logic operations in fluidics as foundation for embedded biohybrid computation. *Device*, 1(6), 2023.

[16] Microfluidics for nano-drug delivery systems: From fundamentals to industrialization. *Acta Pharmaceutica Sinica B*, 13(8):3277–3299, 2023.

[17] Masashi YOKOTA Ryuto YOSHIDA, Wataru KOBAYASHI. Analysis of design parameters of aqua drive fluidics using openfoam. *The Japan Fluid Power System Society*, 2024 (In Japan).

[18] Barna Becsek, Leonardo Pietrasanta, and Dominik Obrist. Turbulent systolic flow downstream of a bioprosthetic aortic valve: velocity spectra, wall shear stresses, and turbulent dissipation rates. *Frontiers in physiology*, 11:577188, 2020.